Chemically induced senescence prompts functional changes in human microglia-like cells

[1]Armanville S. *, [1]Tocco C.*, [1]Haj Mohamad Z., [2]Clarke D., [2,3,4]Robitaille R. and [1,3,4]Drouin-Ouellet J.

[1]Faculté de Pharmacie, Université de Montréal, Montréal, Québec, Canada.
[2]Département de Neurosciences, Université de Montréal, Montréal, Québec, Canada.
[3]Groupe de Recherche sur le Système Nerveux Central (SNC), Université de Montréal, Montréal, Québec, Canada.
[4]Centre Interdisciplinaire de Recherche sur le Cerveau et l'apprentissage (CIRCA), Montréal, Québec, Canada.

Lead contact: janelle.drouin-ouellet@umontreal.ca

*Equal contribution

Running title: Senescence induces functional changes in microglia

Keywords: Cell senescence, aging, human microglia, neuroinflammation, neurodegeneration

Abstract

In response to various stressors, cells can enter a state called cellular senescence which is characterized by irreversible cell cycle arrest and a senescence-associated secretory phenotype (SASP). The progressive accumulation of senescent glial cells in the central nervous system (CNS) with aging suggests a potential role for senescence as driver of aging and inflammation in the brain. As the main immune cell population residing in the CNS, microglia are thought to play a pivotal role in the progression of age-associated neuroinflammation. Furthermore, due to their slow turnover, microglia are highly susceptible to undergoing cellular senescence. However, current understanding of age-related changes in microglia and their impact on brain aging is limited. Due to the challenge in accessing human primary microglia and the lack of models to adequately recapitulate aging, this knowledge is predominantly limited to rodent studies. Here, we chemically induced senescence in a human immortalized microglia cell line with a cocktail of senescence inducing molecules. We demonstrate that chemically induced senescent microglia adopt a pro-inflammatory phenotype, have reduced phagocytic activity and impaired calcium activity. Our results show that chemically induced senescence can mimic features of cellular aging and can provide insight on the impact of aging and cellular senescence on human microglia.

Introduction

A growing number of studies suggests that cellular senescence, primarily characterized by permanent cell cycle arrest, is involved in cellular aging. Senescent cells play a crucial role in wound healing, tissue repair and tumor suppression (1). However, progressive accumulation of senescent cells correlates with the advancement of age (2), suggesting that this biological process could be a driver of aging. This hypothesis has prompted the development of genetic and pharmacological strategies to eliminate senescent cells in an effort to revert signs of aging in the surrounding environment (3). For instance, the depletion of cells expressing the cell senescence marker $p16^{INK4a}$ in the brain of older mice delays loss of cognitive function (4). Unlike apoptotic cells, senescent cells maintain an active metabolic state, known as senescence-associated secretory phenotype (SASP). Cells in this state are characterized by gene expression modifications and secretion of pro-inflammatory cytokines that in turn activate the immune system and allow the clearance of senescent cells (5).

In the brain, the accumulation of senescent cells during aging suggests their potential implication in neuroinflammation and the onset and progression of age-related neurodegenerative disorders. In the healthy brain, microglia are the resident immune cells and are essential for proper brain functioning and homeostasis (6). However, microglia adopt a dystrophic morphology in postmortem brain samples from elderly donors (7-9). Additionally, in *in vivo* and *in vitro* mouse studies, microglia show defective functionality including reduced surveillance and phagocytic activity, increased production of reactive oxygen species (10, 11), reduced response to insults (12), slower migration to sites of infection and processes shrinkage (13). Further, microglia in older mouse brains show more sustained inflammatory response, which correlates with the highly proinflammatory microenvironment characteristic of the aging brain (11). The release of neurotoxic factors, as well as reduced ability to phagocytize cell debris and toxic protein aggregates create an environment that can be harmful to neurons (10, 14). However, the causes of microglial dysfunction with age are poorly described. Recent studies on the aging mouse brain have reported the existence of $p16^{high}$ microglia, suggesting senescence could play a role in age-related microglial dysfunction (15-17).

In humans, dystrophic microglia have been reported in postmortem brain tissues of patients affected by various neurodegenerative diseases. For example, they have been detected near accumulation sites of the tau protein and beta-amyloid plaques in Alzheimer's disease (AD), as well as near Lewy bodies in

cases of dementia with Lewy bodies (18-20). Additionally, a state of intense microglial activation has been observed in mouse models of Parkinson's disease (PD), as well as human postmortem samples from PD patients (21, 22). Thus, even though microglial activation is primarily a neuroprotective defense mechanism, its aberrantly sustained activation is suspected to contribute to neuroinflammation in age-related neurodegenerative disorders (23).

To date, only a handful of studies has been conducted on aged human microglia (9, 13, 24, 25). This is likely due to the limited accessibility of these cells, and the lack of non-invasive imaging tools that would allow the study of living aged microglia at the molecular level (26). Therefore, our current understanding of age-related phenotypic changes in microglia stems mainly from studies carried out in mice, as well as in human postmortem brains which do not allow mechanistic studies. However, inter-species differences in lifespans, phenotypes and age-related changes in microglial function may limit the translatability of rodent findings to human microglia and their contribution to brain aging and neurodegenerative diseases (13, 27, 28).

To dissect the role of aging and cellular senescence on human microglia, we report a model in which cellular senescence can be induced in microglia-like cells *via* the exposure to chemicals targeting multiple homeostatic pathways. We show that, compared to non-treated microglia, cells exposed to the small molecule cocktail exhibit classical markers of cellular senescence, adopt a pro-inflammatory phenotype, have reduced phagocytic activity and impaired calcium activity.

Experimental procedures

Cell line and culture

Immortalized human microglial HMC3 cells were cultured in Eagle's Minimum Essential Medium (EMEM) supplemented with 10% fetal bovine serum (FBS) and 100U/mL of penicillin/streptomycin solution (P/S) at 37°C and in 5% CO_2. When cells reached 80-90% confluence, they were trypsinized by incubation with Trypsin-EDTA for 5 min, then collected in fresh complete medium. After centrifuging the cell suspension at 400G for 5 min at room temperature (RT), the supernatant was discarded, and the remaining pellet resuspended in culture medium. Viable cell number was assessed using a Hausser Scientific™ Bright Line™ Counting Chamber and cells were seeded on plastic multi-well culture plates

coated with Gelatin 0.1% for 1h at 37°C. For all material and reagent catalog numbers, refer to **Suppl. Table 1**.

Chemical induction of senescence

The chemical compounds SBI-0206965, O-151 and Lopinavir (29) were prepared in dimethyl sulfoxide (DMSO) to obtain a stock concentration of 10 mM, 1 mM and 1 mM, respectively and stored at -80° C. HMC3 cells were seeded at a density of 2,630 cells/cm^2 on 6, 12, or 24-well plates. After 24h, cells were treated for 6 consecutive days with a cocktail of SBI-0206965 10 µM, O-151 1 µM Lopinavir 1 µM, or with an equivalent concentration of DMSO in standard HMC3 medium. On day 6, cells were trypsinized and seeded at a density of 14,285 cells/cm^2 in 12-well plates to assess phagocytic activity, 8,500 cells/cm^2 in 8-well, glass-bottomed microchambers for calcium imaging, 45,450 cells/cm^2 in 48-well plates for inflammatory stimulation or 2,725 cells/cm^2 for immunostaining analyses.

β-Galactosidase activity

HMC3 cells were fixed in 4% paraformaldehyde (PFA) for 15 min, and β-Galactosidase (β-Gal) activity assessed using the CellEvent™ Senescence Green Detection Kit, according to manufacturer's instructions. Briefly, HMC3 cells were incubated in a solution containing the β-Gal probe diluted 1:1000 in the provided buffer, for 3h in the dark at 37°C. Fluorescent images of 1665px by 1665px were acquired with a Nikon AX/AX R with NSPARC confocal microscope equipped with a 20x lens (PLAN APO 20x DIC M/N2). Positive cells were detected using NIS-Elements analysis software based on β-Gal fluorescence intensity. The percentage of β-Gal positive cells was then calculated by dividing the number of β-Gal positive cells over the total number of cells, identified using 4',6-diamidino-2-phenylindole (DAPI) nuclear labeling.

TUNEL ASSAY

One day following SLO treatment, HMC3 cells were fixed as previously mentioned, and apoptosis was assessed using the Click-IT TUNEL Alexa Fluor™ Imaging Assay, according to the manufacturer's instructions. Briefly, cells were incubated with an enzyme that incorporate modified deoxyuridine triphosphate to 3'-OH ends of fragmented DNA and the fluorescent detection is based on a click reaction that allows to identify fragmented DNA, a hallmark of apoptosis. DNase I, provided in the kit, was used to induce strand breaks in the DNA and was used as a positive control for TUNEL reaction.

Immunocytochemistry

One day following the SLO treatment, cells were fixed as previously mentioned. For ICC, cells were permeabilized and blocked in a solution containing 0.1% Triton-X-100 and 5% donkey in 0.1M PBS for 30 min. For p21, γH2AX, Lamin B1, pHH3 and HMGB1 staining, cells were permeabilized and blocked in a solution containing 0.2% Triton-X-100 and 3% bovine serum albumin (BSA) in 0.1M PBS for 1h. Primary antibodies (**Suppl. Table 2**) were diluted in permeabilization/blocking solution and applied overnight at 4°C. After PBS 1X rinsing, samples were incubated with Fluorophore-conjugated secondary antibodies and DAPI (1:1000), previously diluted in permeabilization/blocking solution, for 2h, at RT and protected from light. Then, samples were rinsed 3 times with PBS 1X prior to imaging. Fluorescent images of 1665px by 1665px and 356px by 356px were acquired with a Nikon AX/AX R with NSPARC confocal microscope equipped with a 20x lens (PLAN APO 20x DIC M/N2). Nucleus area, defined as the DAPI-stained region, was determined using NIS-Elements analysis software (Nikon) and represented in px^2. Number of γH2AX foci per cell, was measured as number of γH2AX-positive spots detected within each DAPI-stained region.

Pro-inflammatory stimulation and cytokine secretion analysis

24h after plating, cells were stimulated with a solution of lipopolysaccharide (LPS; 100 ng/mL) and interferon-γ (IFNγ; 10 ng/mL) in standard HMC3 medium for 6h (30). Then, culture medium was collected for ELISA, whereas adherent cells were either processed for RNA extraction and further analyzed by qPCR or fixed for ICC analysis. Post stimulation media were further supplemented with protease inhibitors, centrifuged at 300G for 5 min at 4°C to remove cellular debris and processed as per manufacturer's instructions to assess secretion of cytokines interleukin 6 (IL-6) and 8 (IL-8), as well as tumor necrosis factor α (TNFα) and interleukin IL-1β. Absorbance was read at 450 nm using a SYNERGY H1 microplate reader, then corrected using the average absorbance values read at 540 and 570 nm.

RT-qPCR

HMC3 cells were collected and centrifuged at 400G for 5 min at RT. The supernatant was discarded, and samples were kept at -80°C until further processing. RNA extraction was carried out following the RNeasy MicroKit protocol and RNA concentration measured using a Nanodrop spectrophotometer. cDNA was synthesized from the extracted RNA using the SuperScriptTM VILO™ Mastermix. ACTB and

HPTR1 genes were used as housekeeping genes. The relative expression of genes of interest was determined by quantitative polymerase chain reaction (qPCR) using PowerUp™ SYBR™ Green Master Mix. Data were quantified using the ΔΔCT method. For a list of primers used in this study, refer to **Suppl. Table 3**.

Assessment of phagocytotic capacity by flow cytometry

24h after reseeding, HMC3 cells were incubated with 0.75µm fluorescent carboxylate microspheres for 4h in standard HMC3 medium. Phagocytic capacity was then determined using the CytoFLEX Flow Cytometer instrument and measured as percentage of YFP positive cells. Cells not exposed to beads served as a control to determine the target population based on size. Analysis was performed with the CytExpert software.

Calcium imaging

24h after reseeding, HMC3 cells were loaded for 1h with the membrane-permeant Ca^{2+} probe Fluo-4 AM by replacing standard HMC3 medium with loading medium (1 µM Fluo-4 AM, 0.02% Pluronic acid and 1% DMSO, dissolved in standard HMC3 medium). Then, cells were rinsed twice in PBS 1X to remove any Fluo-4 AM residual and let rest in standard medium condition for 20 min prior to recording. Recording was then carried out in PBS 1X with Ca^{2+} and Mg^{2+}, without phenol red. Fluorescent images of 2048px by 2048px (1746 µm by 1746 µm) fields of view were acquired with a Nikon AX/AX R with NSPARC confocal microscope equipped with a 10x lens (PLAN APO λD 10x OFN25 DIC N1). 360 frames were recorded at 1Hz. Specifically, the initial 120 frames before ATP administration were used to define baseline activity, whereas the following 240 frames recorded calcium dynamics elicited by 100nM ATP administration. NIS-Elements software was used to segment single cells and extract signal intensity traces for each individual region of interest (ROI). Each ROI trace was normalized by subtracting background signal intensity values and by dividing by the relative average baseline signal intensity.

Among all recorded cells (N= 433 and N= 83 for control VEH and SLO treated conditions, respectively), only cells showing a foldchange at maximum peak of at least 2 from baseline (N = 156; 36% and N= 58; 70% for control VEH and SLO treated conditions, respectively) were included in the analyses. Extrapolation of 90%/10% decay time, peak time, peak amplitude, and area under the curve (AUC) measurements was performed with ClampFit 10.7 open-source software. For time-lapse of microglial calcium imaging, refer to **Suppl. videos S1 and S2**.

Statistical analyses

GraphPad Prism 10 software was used for statistical analysis. Shapiro-Wilk normality test was used to assess the normality of the distribution. When normality could not be assumed, a nonparametric test was performed. Groups were compared using either Bonferroni's one-way multiple comparison ANOVA, Kruskal-Wallis test with Dunn's multiple comparisons tests or Bonferroni's two-way multiple comparison ANOVA. Unpaired Student's t-test was used in the case of a two-group comparison. An alpha level of 0.05 was defined for significance.

Results

Exposure to SLO leads to a senescent-like phenotype in microglia

A recent study identified a combination of three small molecules capable of inducing senescence in neurons differentiated from iPSCs (29). These molecules include an autophagy inhibitor (SBI-020695), a DNA glycosylase inhibitor (O-151) and an HIV protease 1 inhibitor (Lopinavir). In the study, SLO treated neurons shared features of cells in the aged cortex and presented age-related transcriptional alteration comparable to aged human brain tissues (29). Here, we generated a model of aged human microglia *via* administration of SLO molecules to immortalized human microglia. To determine the minimum effective dose, cells where exposed for 6 consecutive days to either the full dose as reported by Fathi and colleagues (SLO), or a half dose (SLO ½). Control cells were treated with equivalent concentrations of DMSO (vehicle; VEH). First, we assessed whether exposure to the small molecules was inducing apoptosis-induced cell death. No induction of cell death could be observed using a TUNEL assay (**Fig. 1a**). Next, considering that cell cycle arrest is one of the main characteristics of cellular senescence (31), we measured cell proliferation by quantifying the percentage of cells positive for the mitosis marker phosphorylated histone 3 (pHH3). There was a significant reduction of proliferation in the SLO full dose, but not SLO ½, compared to the vehicle condition (**Fig. 1b,c**). In a similar fashion, levels of the cell cycle arrest marker p21 were significantly increased compared to vehicle (**Fig. 1d,e**). Interestingly, senescent-associated morphological changes such as an increase in nucleus area, a disruption of shape, invaginations and an enlargement or fragmentation of the nucleus (32-35) could be observed in the nucleus of SLO treated cells (**Fig. 1e,f**). Since senescent and aged cells are reported to accumulate double-strand DNA damage (36-38), we next assessed whether SLO could induce such accumulation in HMC3 cells. For this purpose, we performed immunocytochemistry against γH2AX, a marker of DNA

damage (39) and quantified the number of γH2AX foci per nucleus in VEH and SLO treated cells. Our results show that SLO full dose, but not half dose, significantly induces double-strand DNA damage, compared to vehicle controls (**Fig. 1e,g**). Similarly, only microglia treated with the full dose of SLO showed increased activity of lysosomal enzyme β-Gal (**Fig. 1h,i**), characteristic of senescence cells. Next, we looked at HMGB1 expression following the SLO treatment. Extracellular HMGB1 acts as a damage-associated molecular pattern (DAMP) molecule which induces inflammation to the site of tissue damage (40, 41). However, under normal conditions, HMGB1 is localized in the nucleus as a chromatin associated non-histone binding protein (42). In senescent cells, HMGB1 translocates from the nucleus to the cytoplasm to be secreted (43) and it modulates senescence by binding to the surface of immune cells to initiate the signaling pathway responsible for the expression of pro-inflammatory cytokines (40). Our results show a significant decrease of nuclear HMGB1 accompanied by an increase in secreted HMGB1 (**Fig. 1j-l**), suggesting that it was mostly secreted to mediate SASP. Finally, Lamin B1, an important structural component of the nuclear lamina, implicated in modulation of nuclear functions and whose expression decreases in senescent cells (44), was decreased in SLO treated cells (**Fig. 1l,m**). Together, our results indicate that a SLO full-dose regimen, while not showing cell apoptosis, is sufficient to induce multiple features of cellular senescence in HMC3 cells. As such, subsequent experiments were conducted with the full dose of SLO only.

Exposure to SLO leads to SASP, decreased phagocytotic activity and slower calcium activity

With age, microglial homeostatic function is thought to become increasingly disrupted over time, a process that is deemed to be implicated in the progression of neurodegenerative diseases (10, 23, 45). Thus, we sought to investigate whether SLO-treated microglia would adopt a proinflammatory profile. SLO- and vehicle-treated cells were exposed for 6 hours to either a combination of the proinflammatory stimuli LPS and IFNγ (LPS/IFNγ), or vehicle (CTL). After the proinflammatory stimulation, the gene expression of common inflammatory cytokines IL-1β, IL-6, IL-8 and TNF was assessed by RT-qPCR and protein secretion in the supernatant by ELISA. In line with our hypothesis, the transcript expression of all cytokines was significantly increased upon pro-inflammatory stimulation in SLO-treated microglia compared to control vehicle. Among them, IL-1β was the only cytokine to show a higher relative expression already at basal levels (**Fig. 2a**). In line with our RT-qPCR results, both IL-6 and IL-8 showed increased secretion post-stimulation in SLO treated cells, compared to control (**Fig. 2b**), but secretion of IL-1β and TNFα was not detected in any of the conditions. According to literature, HMC3 cells are unable

to secrete TNFα (31) whereas the expression of IL-1β has been verified at both mRNA and protein level by western blot, but its secretion in the media remains elusive, possibly due to high turnover rate of the mature protein (42, 43). Importantly, secretion of both IL-6 and IL-8 was increased at baseline in SLO-treated cells, in line with the senescent-like profile exhibited by these cells (**Fig. 2b**).

In addition to the pro-inflammatory secretion profile, aged microglia have been reported to show impairment of phagocytic capacities (46-48). To test if SLO caused similar defects, we evaluated phagocytic activity of control and senescent microglia by measuring intake efficiency of fluorescent beads over a 3h period. Our results show a 10-fold decrease of bead intake in SLO-treated cells compared to vehicle-treated cells (**Fig. 2c,d**), pointing towards decreased phagocytic capacities in chemically induced senescent microglia. Finally, to further characterize the effects of the SLO cocktail on microglia function, we tested whether intracellular calcium (Ca^{2+}) dynamics were altered upon SLO administration. In physiological conditions, dynamics of intracellular calcium are known to modulate several properties and functions of microglia, including proliferation and phagocytosis (49). Further, a recent study conducted in the aging mouse brain reported impairment in *in vivo* Ca^{2+} activity in microglia compared to young and middle-aged brains (50). Upon 30 min incubation with Fluo4-AM fluorescent calcium indicator, cells were recorded over the course of 6 min, including 2 min of baseline activity, and 4 min of activity post ATP stimulation (**Fig. 2e**). Interestingly, while there was a trend towards a higher percentage of cells responding to ATP stimulation in the SLO condition (**Fig. 2f**), SLO treated cells depicted slower calcium dynamics, with longer decay time (**Fig. 2g**), delayed peak time (**Fig. 2h**) and increased AUC (**Fig. 2j**) compared to control cells, while peak amplitude remained similar (**Fig. 2i**). Together, our results show that microglia cells treated with the senescence inducing cocktail SLO acquire features of aging microglia such as increased immunoreactivity, reduced phagocytosis capacities and aberrant calcium dynamics.

Discussion

The goal of this study was to develop a model that better recapitulates the impact of aging and cellular senescence on human microglial functions. We found that the chemical induction of cellular senescence with the SLO cocktail in HMC3 cells rapidly induces characteristics of aged microglia. Induction of cellular senescence in microglia-like cells was confirmed by a reduction of cellular proliferation, an increase of β-Gal activity, p21 protein level, accumulation or γH2AX foci, decreased HMGB1 expression in the

nucleus leading to its secretion, decreased expression of Lamin B1 and nucleus area. Further, senescent microglia-like cells adopted a pro-inflammatory phenotype which was accompanied by reduced phagocytic activity and impaired calcium activity.

Mechanisms of action of the three different molecules used to induce cellular senescence highlight potential pathways that could drive cellular senescence in aged microglia. Accumulation of damaged mitochondria has been reported in senescent cells and is thought to be a driving mechanism of cellular senescence (51, 52). In our paradigm, the use of SBI-0206965, a known inhibitor of the autophagy initiator kinase ULK1, leads to dysfunctional autophagosomes and ultimately affects clearing of damaged mitochondria. Additionally, the inhibition of autophagy can lead to aggregation of oxidized proteins, carbonyls proteins and products of lipidic peroxidation and protein glycation found in lipofuscin granules which are also observed in the cytoplasm of senescent cells (53, 54). Cytoplasmic lipofuscin accumulation has also been observed in senescent cells, highlighting the relevance of autophagy dysfunction in driving cellular senescence (54, 55). Recent studies have revealed SBI-0206965 also functions as an inhibitor of AMP-activated protein kinase (AMPK), in a more specific fashion than dorsomorphin, the most used AMPK inhibitor (56). It has been demonstrated that dorsomorphin can be used to efficiently cause features of senescence in microglia. Interestingly, the use of dorsomorphin causes disruption of microglial functions similarly to SLO treatment, including higher levels of pro-inflammatory cytokines production and reduction of phagocytosis (57). These data raise the possibility that exclusively inhibiting autophagy via SBI-0206965 could be sufficient to induce cellular senescence in microglia-like cells, but further experiments are required. Next, the molecule O-151 is a known inhibitor of the 8-oxoguanine DNA-glycosylase, a key component of the major pathway implicated in the repair of oxidative DNA damage (58). Previous evidence demonstrates that efficiency of DNA repair systems declines with age which could explain the accumulation of age-associated DNA damage (37, 59, 60). The correlation of high levels of reactive oxygen species with age reflects the relevance of targeting the most common oxidative DNA lesion repair process to induce features of aging (61). Finally, the impact of Lopinavir, an HIV protease 1 inhibitor, in the induction of cellular senescence is related to its role in disrupting Lamin A processing and leading to progeria-like features in treated cells and patients (62). Mature Lamin A, a component of the nuclear lamina, is normally generated by the cleavage of pre-Lamin A by a zinc metalloprotease, ZMPSTE24 (63). However, this enzymatic activity can be blocked by Lopinavir, leading to accumulation of pre-Lamin A and premature aging (64). Fathi and

colleagues used these three molecules to induce features of cellular senescence stem-cell derived motor neurons, suggesting that these targeted pathways are important in neuronal health and neurodegenerative diseases (29). Adult microglia retain a low rate of proliferation, to ensure the preservation of their homeostatic population in relatively constant numbers (28). In this study, we show that the SLO molecules induce cell cycle arrest, a feature that was not assessed in neurons treated with SLO given that neurons are post-mitotic.

In the healthy brain, microglial cells ensure CNS homeostasis by constantly monitoring the presence of endogenous and exogenous harmful substances in their microenvironment. For this purpose, these cells are in continuous movement to cover long distances and monitor large areas of the brain (65). As such, they exhibit dynamic behavior characterized by the ability to quickly switch to an activated state and adopt anti- or pro-inflammatory phenotypes upon detection of danger (65). However, with age, microglial homeostatic functions are gradually disrupted. Possibly due to previous exposure to harmful factors, aging microglia are often reported as being primed or reactive, and can respond in a more robust and sustained manner to an insult (65, 66), while showing reduced phagocytosis activity (67). Similar functional changes are also reported in senescent microglia induced by increased proliferation in a mouse model of AD (68), suggesting cellular senescence could constitute a common source of age-related functional alterations in the context of neurodegenerative disease. However, the mechanisms through which senescence affects cellular function remain elusive. It has been proposed that changes in the homeostatic genes expression profile that occurs with age could explain these phenotypical changes (10). Age-related sustained microglial activation could also be explained by the enhancing effect of SASP components, namely IL-6 and IL-8 (69). In this study, both cytokines are released upon SLO treatment. It has been reported that SASP factors can reinforce senescence in both autocrine and paracrine fashion. In this context, the use of co-cultures of microglia and neurons would help to elucidate the role of senescence in brain aging. Some evidence suggests that with age, neurons adopt senescence-like phenotype and studies conducted in rodents showed that neurons can acquire a SASP-like phenotype and induce premature paracrine senescence in embryonic fibroblasts (70, 71). Co-cultures of neurons and microglia could provide additional insight in this regard.

Analysis of calcium activity in microglia has been used to study their state of activation, as intracellular calcium signaling allows to coordinate and perform microglial executive functions (72). Results from a

study conducted in mice revealed age-related changes in intracellular calcium signaling (50). In this paper, the authors identified in middle-aged mice a subpopulation of microglia showing a more reactive phenotype and characterized by increased spontaneous calcium transients. This population of cells was more abundant than in young animals. Interestingly, this phenomenon was further exacerbated in old mice, where another microglia subpopulation characterized by a more senescent or dysfunctional phenotype was reported, with faster migration of microglial processes toward ATP-sources albeit in a more disorganized manner (50). In our work, we show that although SLO-treated cells still display robust calcium activity in response to ATP, they exhibit calcium dynamics distinct from VEH-treated cells. This could have an impact on phagocytosis proficiency, cellular motility, and the metabolic state of SLO-treated microglia. However, a clear link between dysfunctional calcium signaling and microglial functions in our system has yet to be determined.

Despite presenting obvious advantages such as easy and reproducible handling and a high rate of proliferation, the use of immortalized cell lines is a limitation to study the effects of aging and senescence on cellular functions. HMC3 cells were generated via immortalization of human microglia by SV40T transfection (73). Despite retaining most of the characteristics of normal cells, some properties can be affected. For instance, HMC3 cells display lower phagocytic activity than primary microglia (30) and some studies also reported that expression the inflammatory mediators IL-1β, IL-6, TNFα, iNOS, VEGF and TGFβ1 could only be confirmed at the mRNA levels but were not observed at the protein level (30, 74, 75), as we also report in our work (**Fig. 2a,b**). Finally, HMC3 immortalization process also altered some microglial original antigenic characteristics, such as the loss of expression at basal level of CD68 and CD11b, two markers of activated microglia (30). Moving forward, the use of iPSC-derived microglia would be a preferred human microglial model, as it more closely resembles primary microglia. However, immortalized cells tend to be easier to culture than primary cultures and have been modified to proliferate indefinitely suggesting that SLO concentrations would certainly need to be adjusted to induce cellular senescence while avoiding toxicity and induction of cellular death.

Taken together, we present a new model of chemically induced senescence in microglia-like cells and show the impact of this phenotypic change on phagocytic and calcium activity. The combination of a renewable source of microglia, with a reliable protocol to induce cellular senescence will help gain

insight on the potential role of microglial senescence in the aging brain and the progression of neurodegenerative disorders.

Acknowledgements

We thank Nicolas Giguère (University of Montreal) for his valuable help with high content imaging. This project has been made possible by the Brain Canada Foundation through the Canada Brain Research Fund with the financial support of Health Canada and the Azrieli Foundation as well as by funding from the Canada Research Chair Program to J.D.O. C.T is receiving a Postdoctoral fellowship from Parkinson Canada. Z.H.M received a Natural Science and Engineering Research Council undergraduate scholarship.

References

1. Serrano M. Senescence helps regeneration. Dev Cell. 2014;31(6):671-2.
2. Khosla S, Farr JN, Tchkonia T, Kirkland JL. The role of cellular senescence in ageing and endocrine disease. Nat Rev Endocrinol. 2020;16(5):263-75.
3. Zhang X, Englund DA, Aversa Z, Jachim SK, White TA, LeBrasseur NK. Exercise Counters the Age-Related Accumulation of Senescent Cells. Exerc Sport Sci Rev. 2022;50(4):213-21.
4. Zhang X, Pearsall VM, Carver CM, Atkinson EJ, Clarkson BDS, Grund EM, et al. Rejuvenation of the aged brain immune cell landscape in mice through p16-positive senescent cell clearance. Nat Commun. 2022;13(1):5671.
5. Baker DJ, Wijshake T, Tchkonia T, LeBrasseur NK, Childs BG, van de Sluis B, et al. Clearance of p16Ink4a-positive senescent cells delays ageing-associated disorders. Nature. 2011;479(7372):232-6.
6. Borst K, Dumas AA, Prinz M. Microglia: Immune and non-immune functions. Immunity. 2021;54(10):2194-208.
7. Neumann P, Lenz DE, Streit WJ, Bechmann I. Is microglial dystrophy a form of cellular senescence? An analysis of senescence markers in the aged human brain. Glia. 2023;71(2):377-90.
8. Streit WJ. Microglial senescence: does the brain's immune system have an expiration date? Trends Neurosci. 2006;29(9):506-10.
9. Streit WJ, Sammons NW, Kuhns AJ, Sparks DL. Dystrophic microglia in the aging human brain. Glia. 2004;45(2):208-12.
10. Yoo HJ, Kwon MS. Aged Microglia in Neurodegenerative Diseases: Microglia Lifespan and Culture Methods. Front Aging Neurosci. 2021;13:766267.
11. Grabert K, Michoel T, Karavolos MH, Clohisey S, Baillie JK, Stevens MP, et al. Microglial brain region-dependent diversity and selective regional sensitivities to aging. Nat Neurosci. 2016;19(3):504-16.
12. Butovsky O, Weiner HL. Microglial signatures and their role in health and disease. Nat Rev Neurosci. 2018;19(10):622-35.
13. Galatro TF, Holtman IR, Lerario AM, Vainchtein ID, Brouwer N, Sola PR, et al. Transcriptomic analysis of purified human cortical microglia reveals age-associated changes. Nat Neurosci. 2017;20(8):1162-71.
14. Wang Y, Cella M, Mallinson K, Ulrich JD, Young KL, Robinette ML, et al. TREM2 lipid sensing sustains the microglial response in an Alzheimer's disease model. Cell. 2015;160(6):1061-71.
15. Talma N, Gerrits E, Wang B, Eggen BJL, Demaria M. Identification of distinct and age-dependent p16(High) microglia subtypes. Aging Cell. 2021;20(10):e13450.
16. Matsudaira T, Nakano S, Konishi Y, Kawamoto S, Uemura K, Kondo T, et al. Cellular senescence in white matter microglia is induced during ageing in mice and exacerbates the neuroinflammatory phenotype. Commun Biol. 2023;6(1):665.
17. Ng PY, Zhang C, Li H, Baker DJ. Senescent Microglia Represent a Subset of Disease-Associated Microglia in P301S Mice. J Alzheimers Dis. 2023;95(2):493-507.
18. Streit WJ. Microglia and Alzheimer's disease pathogenesis. J Neurosci Res. 2004;77(1):1-8.
19. Lopes KO, Sparks DL, Streit WJ. Microglial dystrophy in the aged and Alzheimer's disease brain is associated with ferritin immunoreactivity. Glia. 2008;56(10):1048-60.

20. Streit WJ, Xue QS. Microglia in dementia with Lewy bodies. Brain Behav Immun. 2016;55:191-201.
21. Joers V, Tansey MG, Mulas G, Carta AR. Microglial phenotypes in Parkinson's disease and animal models of the disease. Prog Neurobiol. 2017;155:57-75.
22. McGeer PL, Itagaki S, Boyes BE, McGeer EG. Reactive microglia are positive for HLA-DR in the substantia nigra of Parkinson's and Alzheimer's disease brains. Neurology. 1988;38(8):1285-91.
23. Kwon HS, Koh SH. Neuroinflammation in neurodegenerative disorders: the roles of microglia and astrocytes. Transl Neurodegener. 2020;9(1):42.
24. Olah M, Patrick E, Villani AC, Xu J, White CC, Ryan KJ, et al. A transcriptomic atlas of aged human microglia. Nat Commun. 2018;9(1):539.
25. Lopes KP, Snijders GJL, Humphrey J, Allan A, Sneeboer MAM, Navarro E, et al. Genetic analysis of the human microglial transcriptome across brain regions, aging and disease pathologies. Nat Genet. 2022;54(1):4-17.
26. Wendimu MY, Hooks SB. Microglia Phenotypes in Aging and Neurodegenerative Diseases. Cells. 2022;11(13).
27. Zhang Y, Sloan SA, Clarke LE, Caneda C, Plaza CA, Blumenthal PD, et al. Purification and Characterization of Progenitor and Mature Human Astrocytes Reveals Transcriptional and Functional Differences with Mouse. Neuron. 2016;89(1):37-53.
28. Reu P, Khosravi A, Bernard S, Mold JE, Salehpour M, Alkass K, et al. The Lifespan and Turnover of Microglia in the Human Brain. Cell Rep. 2017;20(4):779-84.
29. Fathi A, Mathivanan S, Kong L, Petersen AJ, Harder CRK, Block J, et al. Chemically induced senescence in human stem cell-derived neurons promotes phenotypic presentation of neurodegeneration. Aging Cell. 2022;21(1):e13541.
30. Janabi N, Peudenier S, Heron B, Ng KH, Tardieu M. Establishment of human microglial cell lines after transfection of primary cultures of embryonic microglial cells with the SV40 large T antigen. Neurosci Lett. 1995;195(2):105-8.
31. Kumari R, Jat P. Mechanisms of Cellular Senescence: Cell Cycle Arrest and Senescence Associated Secretory Phenotype. Front Cell Dev Biol. 2021;9:645593.
32. Swanson EC, Manning B, Zhang H, Lawrence JB. Higher-order unfolding of satellite heterochromatin is a consistent and early event in cell senescence. J Cell Biol. 2013;203(6):929-42.
33. Goldman RD, Shumaker DK, Erdos MR, Eriksson M, Goldman AE, Gordon LB, et al. Accumulation of mutant lamin A causes progressive changes in nuclear architecture in Hutchinson-Gilford progeria syndrome. Proc Natl Acad Sci U S A. 2004;101(24):8963-8.
34. Ivanov A, Pawlikowski J, Manoharan I, van Tuyn J, Nelson DM, Rai TS, et al. Lysosome-mediated processing of chromatin in senescence. J Cell Biol. 2013;202(1):129-43.
35. Scaffidi P, Misteli T. Lamin A-dependent nuclear defects in human aging. Science. 2006;312(5776):1059-63.
36. d'Adda di Fagagna F, Reaper PM, Clay-Farrace L, Fiegler H, Carr P, Von Zglinicki T, et al. A DNA damage checkpoint response in telomere-initiated senescence. Nature. 2003;426(6963):194-8.
37. Lou Z, Chen J. Cellular senescence and DNA repair. Exp Cell Res. 2006;312(14):2641-6.
38. Lombard DB, Chua KF, Mostoslavsky R, Franco S, Gostissa M, Alt FW. DNA repair, genome stability, and aging. Cell. 2005;120(4):497-512.
39. Sedelnikova OA, Rogakou EP, Panyutin IG, Bonner WM. Quantitative detection of (125)IdU-induced DNA double-strand breaks with gamma-H2AX antibody. Radiat Res. 2002;158(4):486-92.
40. Davalos AR, Kawahara M, Malhotra GK, Schaum N, Huang J, Ved U, et al. p53-dependent release of Alarmin HMGB1 is a central mediator of senescent phenotypes. J Cell Biol. 2013;201(4):613-29.

41. Semino C, Angelini G, Poggi A, Rubartelli A. NK/iDC interaction results in IL-18 secretion by DCs at the synaptic cleft followed by NK cell activation and release of the DC maturation factor HMGB1. Blood. 2005;106(2):609-16.
42. Rouillard ME, Hu J, Sutter PA, Kim HW, Huang JK, Crocker SJ. The Cellular Senescence Factor Extracellular HMGB1 Directly Inhibits Oligodendrocyte Progenitor Cell Differentiation and Impairs CNS Remyelination. Front Cell Neurosci. 2022;16:833186.
43. Sofiadis K, Josipovic N, Nikolic M, Kargapolova Y, Ubelmesser N, Varamogianni-Mamatsi V, et al. HMGB1 coordinates SASP-related chromatin folding and RNA homeostasis on the path to senescence. Mol Syst Biol. 2021;17(6):e9760.
44. Shimi T, Butin-Israeli V, Adam SA, Hamanaka RB, Goldman AE, Lucas CA, et al. The role of nuclear lamin B1 in cell proliferation and senescence. Genes Dev. 2011;25(24):2579-93.
45. Wynne AM, Henry CJ, Huang Y, Cleland A, Godbout JP. Protracted downregulation of CX3CR1 on microglia of aged mice after lipopolysaccharide challenge. Brain Behav Immun. 2010;24(7):1190-201.
46. Bliederhaeuser C, Grozdanov V, Speidel A, Zondler L, Ruf WP, Bayer H, et al. Age-dependent defects of alpha-synuclein oligomer uptake in microglia and monocytes. Acta Neuropathol. 2016;131(3):379-91.
47. Caldeira C, Cunha C, Vaz AR, Falcao AS, Barateiro A, Seixas E, et al. Key Aging-Associated Alterations in Primary Microglia Response to Beta-Amyloid Stimulation. Front Aging Neurosci. 2017;9:277.
48. Njie EG, Boelen E, Stassen FR, Steinbusch HW, Borchelt DR, Streit WJ. Ex vivo cultures of microglia from young and aged rodent brain reveal age-related changes in microglial function. Neurobiol Aging. 2012;33(1):195 e1-12.
49. Suzuki H, Franz H, Yamamoto T, Iwasaki Y, Konno H. Identification of the normal microglial population in human and rodent nervous tissue using lectin-histochemistry. Neuropathol Appl Neurobiol. 1988;14(3):221-7.
50. Olmedillas Del Moral M, Asavapanumas N, Uzcategui NL, Garaschuk O. Healthy Brain Aging Modifies Microglial Calcium Signaling In Vivo. Int J Mol Sci. 2019;20(3).
51. Wickens AP. Ageing and the free radical theory. Respir Physiol. 2001;128(3):379-91.
52. Jin K. Modern Biological Theories of Aging. Aging Dis. 2010;1(2):72-4.
53. Davalli P, Mitic T, Caporali A, Lauriola A, D'Arca D. ROS, Cell Senescence, and Novel Molecular Mechanisms in Aging and Age-Related Diseases. Oxid Med Cell Longev. 2016;2016:3565127.
54. McHugh D, Gil J. Senescence and aging: Causes, consequences, and therapeutic avenues. J Cell Biol. 2018;217(1):65-77.
55. Jurk D, Wang C, Miwa S, Maddick M, Korolchuk V, Tsolou A, et al. Postmitotic neurons develop a p21-dependent senescence-like phenotype driven by a DNA damage response. Aging Cell. 2012;11(6):996-1004.
56. Ahwazi D, Neopane K, Markby GR, Kopietz F, Ovens AJ, Dall M, et al. Investigation of the specificity and mechanism of action of the ULK1/AMPK inhibitor SBI-0206965. Biochem J. 2021;478(15):2977-97.
57. Marques L, Johnson AA, Stolzing A. Doxorubicin generates senescent microglia that exhibit altered proteomes, higher levels of cytokine secretion, and a decreased ability to internalize amyloid beta. Exp Cell Res. 2020;395(2):112203.
58. Donley N, Jaruga P, Coskun E, Dizdaroglu M, McCullough AK, Lloyd RS. Small Molecule Inhibitors of 8-Oxoguanine DNA Glycosylase-1 (OGG1). ACS Chem Biol. 2015;10(10):2334-43.
59. Lans H, Hoeijmakers JH. Genome stability, progressive kidney failure and aging. Nat Genet. 2012;44(8):836-8.

60. Meyer JN, Boyd WA, Azzam GA, Haugen AC, Freedman JH, Van Houten B. Decline of nucleotide excision repair capacity in aging Caenorhabditis elegans. Genome Biol. 2007;8(5):R70.
61. Barja G. Updating the mitochondrial free radical theory of aging: an integrated view, key aspects, and confounding concepts. Antioxid Redox Signal. 2013;19(12):1420-45.
62. Eriksson M, Brown WT, Gordon LB, Glynn MW, Singer J, Scott L, et al. Recurrent de novo point mutations in lamin A cause Hutchinson-Gilford progeria syndrome. Nature. 2003;423(6937):293-8.
63. Navarro CL, Cadinanos J, De Sandre-Giovannoli A, Bernard R, Courrier S, Boccaccio I, et al. Loss of ZMPSTE24 (FACE-1) causes autosomal recessive restrictive dermopathy and accumulation of Lamin A precursors. Hum Mol Genet. 2005;14(11):1503-13.
64. Hudon SE, Coffinier C, Michaelis S, Fong LG, Young SG, Hrycyna CA. HIV-protease inhibitors block the enzymatic activity of purified Ste24p. Biochem Biophys Res Commun. 2008;374(2):365-8.
65. Damani MR, Zhao L, Fontainhas AM, Amaral J, Fariss RN, Wong WT. Age-related alterations in the dynamic behavior of microglia. Aging Cell. 2011;10(2):263-76.
66. Norden DM, Godbout JP. Review: microglia of the aged brain: primed to be activated and resistant to regulation. Neuropathol Appl Neurobiol. 2013;39(1):19-34.
67. Galloway DA, Phillips AEM, Owen DRJ, Moore CS. Phagocytosis in the Brain: Homeostasis and Disease. Front Immunol. 2019;10:790.
68. Hu Y, Fryatt GL, Ghorbani M, Obst J, Menassa DA, Martin-Estebane M, et al. Replicative senescence dictates the emergence of disease-associated microglia and contributes to Abeta pathology. Cell Rep. 2021;35(10):109228.
69. Acosta JC, Banito A, Wuestefeld T, Georgilis A, Janich P, Morton JP, et al. A complex secretory program orchestrated by the inflammasome controls paracrine senescence. Nat Cell Biol. 2013;15(8):978-90.
70. Bigagli E, Luceri C, Scartabelli T, Dolara P, Casamenti F, Pellegrini-Giampietro DE, et al. Long-term Neuroglial Cocultures as a Brain Aging Model: Hallmarks of Senescence, MicroRNA Expression Profiles, and Comparison With In Vivo Models. J Gerontol A Biol Sci Med Sci. 2016;71(1):50-60.
71. Moreno-Blas D, Gorostieta-Salas E, Pommer-Alba A, Mucino-Hernandez G, Geronimo-Olvera C, Maciel-Baron LA, et al. Cortical neurons develop a senescence-like phenotype promoted by dysfunctional autophagy. Aging (Albany NY). 2019;11(16):6175-98.
72. Brawek B, Garaschuk O. Monitoring in vivo function of cortical microglia. Cell Calcium. 2017;64:109-17.
73. Dello Russo C, Cappoli N, Coletta I, Mezzogori D, Paciello F, Pozzoli G, et al. The human microglial HMC3 cell line: where do we stand? A systematic literature review. J Neuroinflammation. 2018;15(1):259.
74. Li B, Bedard K, Sorce S, Hinz B, Dubois-Dauphin M, Krause KH. NOX4 expression in human microglia leads to constitutive generation of reactive oxygen species and to constitutive IL-6 expression. J Innate Immun. 2009;1(6):570-81.
75. Jadhav VS, Krause KH, Singh SK. HIV-1 Tat C modulates NOX2 and NOX4 expressions through miR-17 in a human microglial cell line. J Neurochem. 2014;131(6):803-15.

Figures and legends

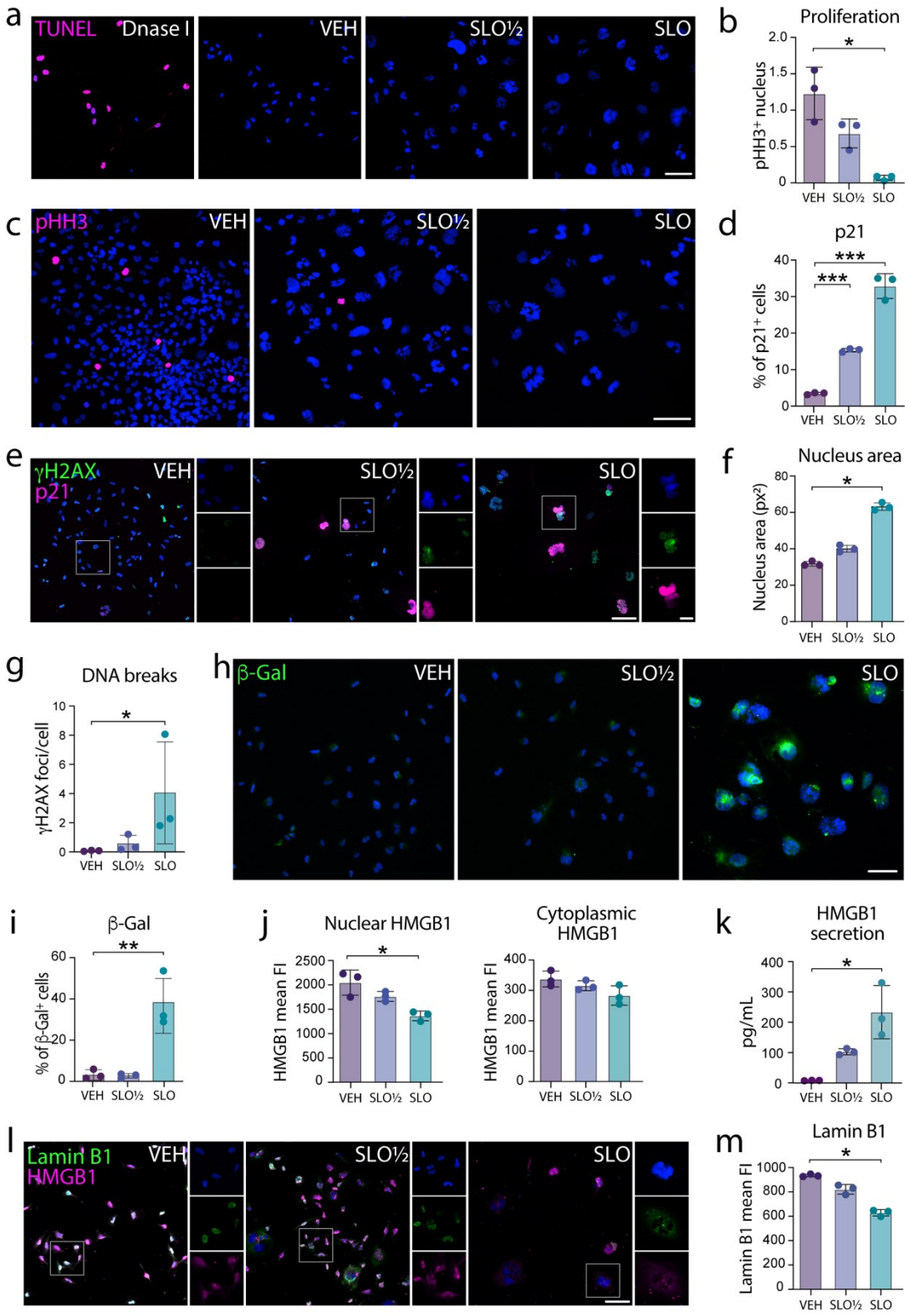

Figure 1. SLO full dose but not half dose induces features of cellular senescence in HMC3 cells. (**a**) Representative fluorescence images showing absence of TUNEL positive cells in VEH, SLO ½ and SLO

treated HMC3 cells, compared to the positive control. (**b**) Cell proliferation quantified as the number of pHH3 positive cells over the total number of cells. (**c**) Representative fluorescence images showing pHH3 positive cells in microglia-like cells treated with VEH, SLO ½ and SLO. DAPI (blue) is used as nuclear counterstaining. (**d**) Quantification of percentage of p21-positive cells over total number of cells. (**e**) Representative fluorescence images showing microglia treated with VEH, SLO ½ and SLO co-stained with p21 and γH2AX. DAPI (blue) is used as nuclear counterstaining. (**f**) Nucleus area determined by core surface area (px^2). Each point corresponds to the mean ± standard deviation of the core area of 15 microglia. (**g**) Number of DNA double-strand breaks measured as number of γH2AX-positive foci per nucleus delineated by DAPI. Each point corresponds to the mean ± the standard deviation of the number of γH2AX foci per nucleus of 15 microglia. (**h**) Representative fluorescence images showing β-Gal positive cells in microglia treated with VEH, SLO ½ and SLO. DAPI (blue) is used as nuclear counterstaining. (**i**) Quantification of percentage of β-Gal-positive cells over total number of cells. (**j**) Quantification of HMGB1 fluorescence intensity in the nucleus and in the cytoplasm. (**k**) Protein concentrations (pg/mL) of HMGB1 secreted in culture medium from microglia treated with VEH, SLO ½ and SLO, measured by ELISA. (**l**) Representative fluorescence images showing microglia treated with VEH, SLO ½ and SLO co-stained with HMGB1 and Lamin B1. DAPI (blue) is used as nuclear counterstaining. (**m**) Quantification of Lamin B1 fluorescence intensity in the nucleus. Data for all graphs are represented as mean ± SD. [*$p<0.05$; [**$p<0.01$; ***$p<0.001$ by one-way ANOVA, n=3 independent experiments]. Scale bar = 100 µm (low magnification) and 20 µm (high magnification).

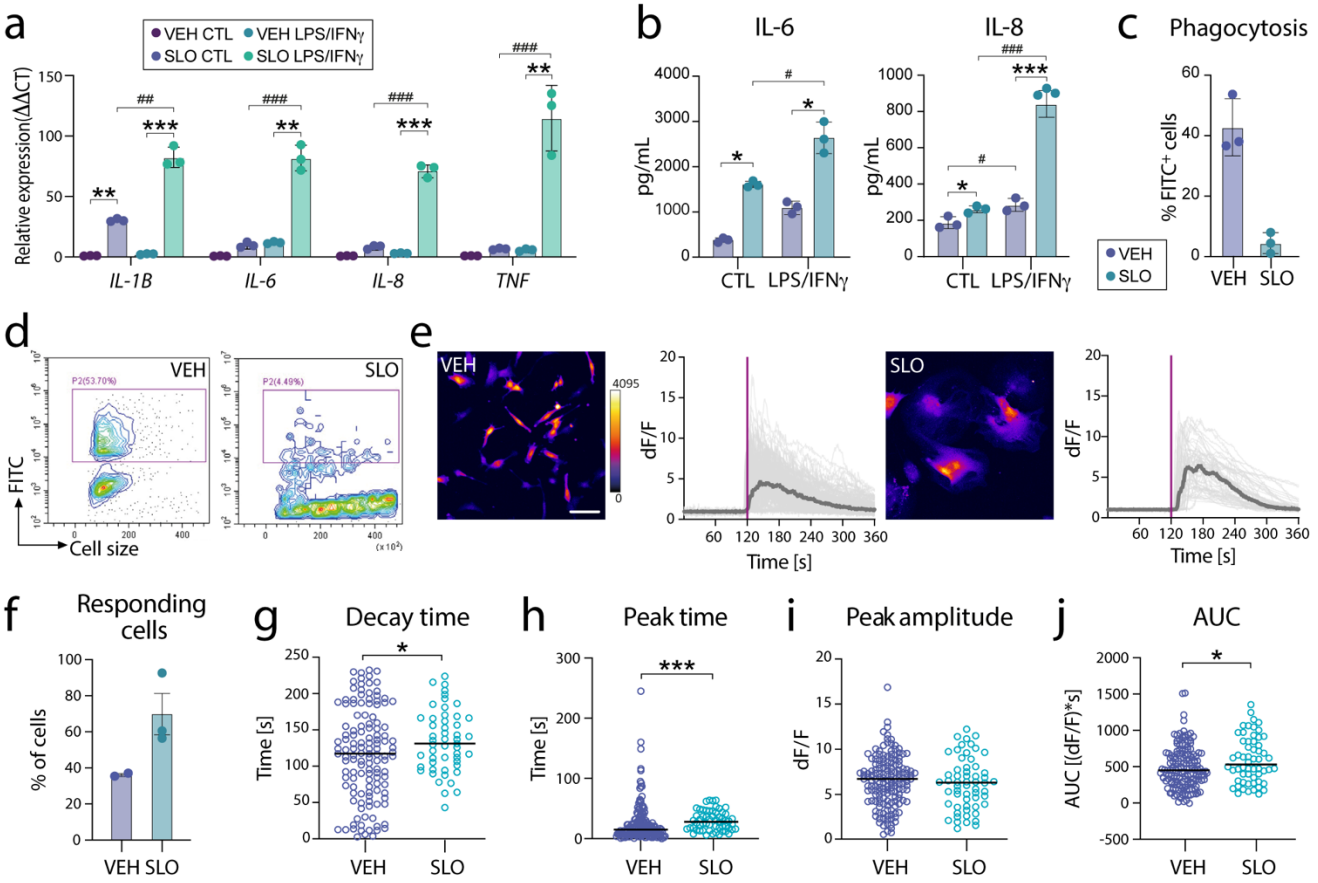

Figure 2. SLO treated HMC3 cells show an overly reactive profile, and aberrant functionality. (**a**) RT-qPCR Quantification of relative gene expression of SASP-associated genes (*IL-1B*, *IL-6*, *IL-8*, *TNF*) in microglia treated with VEH or SLO either stimulated with pro-inflammatory stimulation (LPS/IFNγ) or untreated (CTL). Data are represented as mean ± SD. (**b**) Protein concentration (pg/mL) of IL-6 and IL-8 in culture medium from microglia treated with vehicle (VEH) or senescence molecules (SLO) either stimulated with pro-inflammatory molecules (LPS/IFNγ) or untreated (CTL), measured by ELISA. Data are presented as mean ± SD. (**c**) Flow cytometry analysis showing the incorporation of fluorescein isothiocyanate-labelled (FITC) beads by microglia after treatment with VEH or SLO. Data are presented as mean ± SD. (**d**) Phagocytosis efficiency determined by the percentage of cells that incorporated fluorescent beads. (**e**) Individual cells (light grey) and average traces (dark grey) Ca^{2+} responses elicited by administration of 100nM of ATP (purple line) in control vehicle and SLO treated HCM3 cells. Insets show representative MIP confocal images of the Ca^{2+} level in HMC3 cells loaded with 1µM Ca^{2+} indicator Fluo-4 AM. Representative images of the Fluo-4 AM signal is pseudo colored. (**f**) Quantification of the percentage of cells responding to ATP stimulation. Data are presented as mean ± SD. (**g-j**) Scatter plots showing 90%/10% decay time (**g**), peak time (**h**), peak amplitude (**i**), and area under the curve (AUC, **j**)

measurements for n=156 vehicle- and n=58 SLO-treated cells, collected from N=2 (VEH) and N=3 (SLO) technical replicates. Scale bar = 50µm. [*p<0.05; **p<0.01; ***p<0.001; compared to VEH; #p<0.05; ##p<0.01; ###p<0.001; compared to the CTL group.